J|A|C|S COMMUNICATIONS

Published on Web 12/23/2008

Well-Defined, Multifunctional Nanostructures of a Paramagnetic Lipid and a Lipopeptide for Macrophage Imaging

Esad Vucic,[†] Honorius M. H. F. Sanders,[‡,⊥] Francesca Arena,[§] Enzo Terreno,[§] Silvio Aime,[§] Klaas Nicolay,[‡] Eik Leupold,[∥] Margitta Dathe,[∥] Nico A. J. M. Sommerdijk,[⊥] Zahi A. Fayad,[†] and Willem J. M. Mulder*[,†]

Translational and Molecular Imaging Institute and Imaging Science Laboratories, Mount Sinai School of Medicine, New York, New York 10029, Biomedical NMR, Department of Biomedical Engineering, Eindhoven University of Technology, Eindhoven, The Netherlands, Department of Chemistry IFM and Molecular Imaging Center, University of Torino, Torino, Italy, Leibniz Institute of Molecular Pharmacology, Berlin, Germany, and Soft Matter Cryo-TEM Research Unit, Eindhoven University of Technology, Eindhoven, The Netherlands

Received October 27, 2008; E-mail: willem.mulder@mountsinai.org

In the field of molecular imaging, nanoparticulate structures are becoming increasingly important, since they can carry high payloads of contrast generating materials while their surface can be functionalized to improve biocompatibility or to introduce specificity.[1,2] In addition to inorganic nanocrystals, such as quantum dots (QDs)[3] and iron oxide[4] or gold nanoparticles,[5] self-assembled organic structures including liposomes,[6] micelles,[7] and microemulsions[8] have shown great potential for in vivo imaging. In the field of targeted imaging and therapy the pharmacokinetic profile as well as the tissue penetration potential of the nanovehicles is of paramount importance. Hence, there is a great demand for nanostructures of which the final morphology and size can be judiciously controlled. To this aim, we created a variety of well-defined nanosized supramolecular structures based on two amphiphilic molecules: **Gd-DTPA-DSA**, a Gd^{3+} chelating lipid which exhibits paramagnetic properties for MRI,[6,9] and **P2fA2**, a fluorescein labeled apolipoprotein E derived lipopeptide that has been shown to enhance nanoparticle uptake into rat brain capillary endothelial cells *in vitro*.[10]

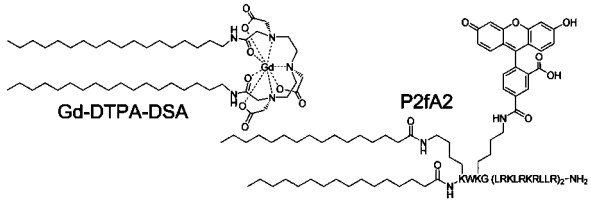

Here we show how we can control the morphology and size of the imaging probes by varying the ratio of the two amphiphiles and thereby optimizing the molecular relaxivity of the resulting lipidic aggregates. The two most effective morphologies were selected for *in vitro* studies and were demonstrated to be effectively internalized by macrophage cells.

Aqueous dispersions of mixtures of **P2fA2** and **Gd-DTPA-DSA** were prepared (Table 1 Supporting Information), and dynamic light scattering (DLS) revealed that the aggregates had narrow size distributions (Supporting Information Figure S1) and that their mean hydrodynamic diameters increased with decreasing **P2fA2/Gd-DTPA-DSA** ratios (Figure 1). At high **P2fA2** contents of 50 mol% or more small structures with a mean diameter below 10 nm were

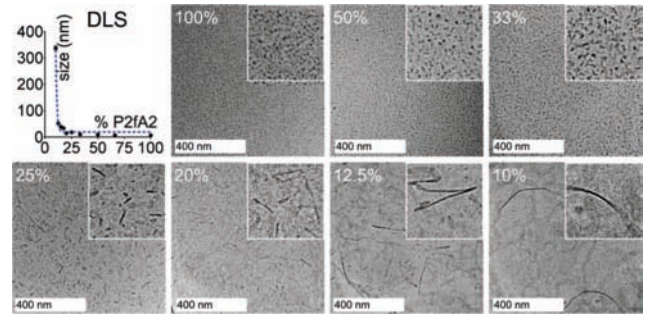

Figure 1. Dynamic light scattering (top, left) and cryo-TEM images of different **P2fA2/Gd-DTPA-DSA** preparations. The insets show a closeup of the cryo-TEM images and represent 200 by 200 nm. The percentages refer to the amount of **P2fA2** in the formulations.

observed, whereas a transition to larger aggregates (8−15 nm) was observed in case the **P2fA2** content was lower than 33 mol%. Below 20 mol% **P2fA2** the mean hydrodynamic diameter increased to ∼60 nm for 12.5 mol% **P2fA2** and to more than 300 nm for a formulation that contained 10 mol% **P2fA2**.

In line with the DLS measurements cryo-TEM revealed aggregates of which the size increased with decreasing **P2fA2** concentration (Figure 1). At **P2fA2** concentrations ≥50 mol% small micellar structures with diameters of 5−8 nm were observed. By decreasing the **P2fA2** concentration plate-like morphologies appeared with a constant thickness of 5−8 nm of which the aspect ratios increased, from by 10 × 15−25 nm (33 mol% **P2fA2**) to 10−15 × 150 nm (25 mol% **P2fA2**) and up to 10−15 × 250 nm (20 mol% **P2fA2**). In the preparations that contained 10−12.5 mol% **P2fA2** fully grown ribbons were present with up to 25 nm in width and with infinite lengths.

Previously, in a study by Johnsson and Edwards it was demonstrated that by carefully mixing regular phospholipids and poly(ethylene glycol) (PEG) conjugated phospholipids a variety of structures, ranging from vesicular, discoidal, to micellar, could be created.[11] The morphological changes were ascribed to the differences in geometry of the amphilphiles used. In our study **Gd-DTPA-DSA** tends to form bilayers with little curvature, while **P2fA2** acts like a strong detergent and curves such that it forms micelles. Therefore aggregates of mixtures of such molecules can have morphologies that are more spherical, plate-like, and even elongated (Supporting Information Figure S2), depending on the ratio of both components.

To assess the applicability of the different nanostructures for magnetic resonance imaging and to characterize their paramagnetic

[†] Mount Sinai School of Medicine.
[‡] Biomedical NMR, Eindhoven University of Technology.
[⊥] Soft Matter Cryo-TEM Research Unit, Eindhoven University of Technology.
[§] University of Torino.
[∥] Leibniz Institute of Molecular Pharmacology.

10.1021/ja808310u CCC: $40.75

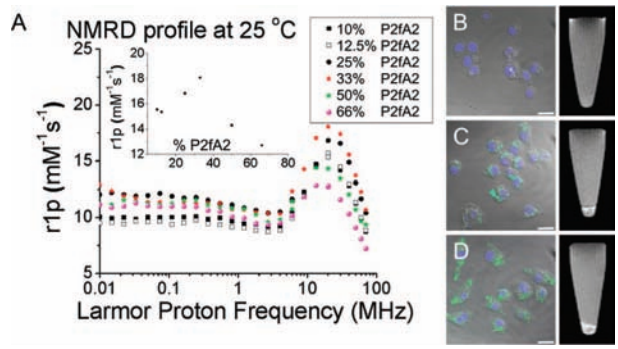

Figure 2. (A) NMRD profiles of the different structures. The inset displays the relaxivity as function of %**P2fA2** at 20 MHz. Confocal microscopy (left) and MRI of loosely packed cell pellets (right) of macrophage cells that were (B) left untreated, incubated with 33% (C) and (D) 50% **P2fA2** nanoparticles. Scale bar: 20 μm.

properties, nuclear magnetic resonance dispersion profiles (NMRD profiles) were obtained (Figure 2). Typical so-called macromolecular profiles with maximum intensities around 20 to 30 MHz were observed. These indicate a diminished mobility of the Gd^{3+} chelates in the lipidic aggregates which causes their tumbling rate τ_R to decrease. This result is typical for supramolecular and macromolecular contrast agents[12] at these moderate, but clinically relevant, field strengths and is not observed for low molecular weight Gd^{3+} chelates. Moreover, these results further support the incorporation of **Gd-DTPA-DSA** in the lipidic aggregates. Our approach allowed the formation of structures with tunable ionic relaxivities, varying between 13 and 18 mM^{-1} s^{-1} at 20 MHz (inset Figure 2), which is 3 to 5 times higher than commercially available Gd-DTPA at this field strength. Interestingly, the highest ionic relaxivity of 18 mM^{-1} s^{-1} was observed for the formulation containing 33% **P2fA2**, the preparation with predominately small plate-like aggregates.

In general such differences in relaxivity are largely determined by the variations in the interplay between the rotation correlation time (τ_R) and the exchange of water molecules coordinated to a single Gd^{3+} chelate. At high **P2fA2** concentrations, i.e., at low local concentrations of **Gd-DTPA-DSA**, it is unlikely that the water exchange rate is the limiting factor. Therefore the observed suboptimal relaxivity at this composition is most likely due to the high τ_R, related to the small aggregate dimensions. Although the aggregate size increases with decreasing **P2fA2** concentrations, a reduction in the relaxivity is observed upon further lowering of the **P2fA2** content past the optimum value of 33 mol%. In this regime, the reduction in ionic relaxivity cannot be related to τ_R, as this parameter is expected to decrease further with the increasing dimensions of the aggregates. Rather, at the concomitant higher Gd-DTPA-DSA concentrations, the water exchange will become a limiting factor and the amount of water that is relaxed per Gd^{3+} chelate will be limiting the ionic relaxivity. Clearly at 33 mol% we find the morphology that optimally benefits from a low rotation correlation time associated with the aggregate dimensions and a Gd^{3+} surface concentration that allows a high enough water exchange rate.

Based on these results we set out to test these **P2fA2** containing nanostructures for their suitability as MR imaging probes for extravascular targets, such as macrophages. Since small nanoparticles are more likely to escape from the circulation and cross the diseased and permeable endothelium, the two formulations with a high relaxivity and small size, *i.e.* those with 33 mol% (small platelets) and 50 mol% (micelles) **P2fA2**, were selected for further *in vitro* experiments with cultured mouse macrophage cells (J774A1). The incorporation of **P2fA2** and **Gd-DTPA-DSA** allowed the visualization of nanoparticle uptake using fluorescence confocal laser scanning microscopy and MRI, respectively (Figure 2). The CLSM images show nuclei in blue (DAPI) and **P2fA2** in green, merged with bright field images of the macrophage cells. While control cells revealed no nanoparticle-associated fluorescence or MRI contrast (Figure 2B), significant amounts of intracellular fluorescence as well as MRI signal enhancement were observed after 30 min of incubation for cells that were incubated with 50% (Figure 2C) and 33% (Figure 2D) **P2fA2** nanoparticles. In addition, we performed quantitative uptake experiments under inhibitory conditions (Supporting Information Figure S3). The results revealed the particle uptake to be specific and further confirmed their multifunctional character.

In summary we have demonstrated that by carefully controlling the ratio of two functional amphiphiles, **Gd-DTPA-DSA** and **P2fA2**, it was possible to create a variety of well-defined supramolecular structures, containing both fluorescein and Gd^{3+} chelates. Moreover, we showed that by changing the morphology we could optimize the relaxivity of the imaging probes, since NMRD profiling disclosed excellent and tunable MRI properties for the different formulations, especially at clinically relevant field strengths.

We envision the application of these contrast agents for pathologies in which macrophage inflammation plays a key role, such as atherosclerosis, rheumatoid arthritis, or cancer.[13]

Acknowledgment. Partial support was provided by NIH/NHLBI R01 HL71021, NIH/NHLBI R01 HL78667 (Z.A.F.) and the DFG (DA 324/5-2 and FG 463, E.L.). David P. Cormode and Heike Nikolenko are gratefully acknowledged for their input.

Supporting Information Available: Figures S1−S3,Table S1, and detailed experimental procedures. This material is available free of charge via the Internet at http://pubs.acs.org.

References

(1) Mulder, W. J.; Strijkers, G. J.; van Tilborg, G. A.; Griffioen, A. W.; Nicolay, K. *NMR Biomed.* **2006**, *19*, 142–164.
(2) Torchilin, V. P. *Nat. Rev. Drug Discovery* **2005**, *4*, 145–160.
(3) Medintz, I. L.; Uyeda, H. T.; Goldman, E. R.; Mattoussi, H. *Nat. Mater.* **2005**, *4*, 435–446.
(4) Bulte, J. W.; Kraitchman, D. L. *NMR Biomed.* **2004**, *17*, 484–499.
(5) Alric, C.; Taleb, J.; Le Duc, G.; Mandon, C.; Billotey, C.; Meur-Herland, A.; Brochard, T.; Vocanson, F.; Janier, M.; Perriat, P.; Roux, S.; Tillement, O. *J. Am. Chem. Soc.* **2008**, *130*, 5908–5915.
(6) Mulder, W. J.; Strijkers, G. J.; Griffioen, A. W.; van Bloois, L.; Molema, G.; Storm, G.; Koning, G. A.; Nicolay, K. *Bioconjugate Chem.* **2004**, *15*, 799–806.
(7) Amirbekian, V.; Lipinski, M. J.; Briley-Saebo, K. C.; Amirbekian, S.; Aguinaldo, J. G.; Weinreb, D. B.; Vucic, E.; Frias, J. C.; Hyafil, F.; Mani, V.; Fisher, E. A.; Fayad, Z. A. *Proc. Natl. Acad. Sci. U.S.A.* **2007**, *104*, 961–966.
(8) Lanza, G. M.; Winter, P. M.; Caruthers, S. D.; Hughes, M. S.; Cyrus, T.; Marsh, J. N.; Neubauer, A. M.; Partlow, K. C.; Wickline, S. A. *Nanomedicine* **2006**, *1*, 321–329.
(9) (a) Mulder, W. J.; Koole, R.; Brandwijk, R. J.; Storm, G.; Chin, P. T.; Strijkers, G. J.; de Mello, D. C.; Nicolay, K.; Griffioen, A. W. *Nano Lett.* **2006**, *6*, 1–6. (b) van Schooneveld, M. M.; Vucic, E.; Koole, R.; Zhou, Y.; Stocks, J.; Cormode, D. P.; Tang, C. Y.; Gordon, R. E.; Nicolay, K.; Meijerink, A.; Fayad, Z. A.; Mulder, W. J. *Nano Lett.* **2008**, *8*, 2517–2525.
(10) (a) Keller, S.; Sauer, I.; Strauss, H.; Gast, K.; Dathe, M.; Bienert, M. *Angew. Chem., Int. Ed.* **2005**, *44*, 5252–5255. (b) Sauer, I.; Nikolenko, H.; Keller, S.; Abu, A. K.; Bienert, M.; Dathe, M. *Biochim. Biophys. Acta* **2006**, *1758*, 552–561. (c) Sauer, I.; Dunay, I. R.; Weisgraber, K.; Bienert, M.; Dathe, M. *Biochemistry* **2005**, *44*, 2021–2029.
(11) Johnsson, M.; Edwards, K. *Biophys. J.* **2003**, *85*, 3839–3847.
(12) Aime, S.; Botta, M.; Terreno, E. *Advances in Inorganic Chemistry - Including Bioinorganic Studies* **2005**, *57*, 173–237.
(13) (a) Libby, P.; Ridker, P. M.; Maseri, A. *Circulation* **2002**, *105*, 1135–1143. (b) Firestein, G. S. *Nature* **2003**, *423*, 356–361. (c) Mantovani, A.; Allavena, P.; Sica, A.; Balkwill, F. *Nature* **2008**, *454*, 436–444.

JA808310U